J Mater Sci: Mater Electron (2021) 32:17115–17122

Degradation analysis with characteristics and simulations of 265 nm UV-C LED

Xinglin Zhu[1], Mengwei Su[1], Zhiqiang Chen[1], Shaodong Deng[1], Huilu Yao[1], Yukun Wang[1], Ziqian Chen[1,*], Jianyu Deng[1,*], and Wenhong Sun[1,2,3,*]

[1] *Research Center for Optoelectronic Materials and Devices, School of Physical Science and Technology, Guangxi University, Nanning 530004, China*

[2] *Guangxi Key Laboratory for Relativistic Astrophysics, School of Physical Science and Technology, Guangxi University, Nanning 530004, China*

[3] *Guangxi Key Laboratory of Processing for Non-Ferrous Metal and Featured Materials, Guangxi University, Nanning 530004, China*

Received: 28 February 2021
Accepted: 3 May 2021
Published online: 22 June 2021

ABSTRACT

We report the degradation study on AlGaN-based 265 nm ultraviolet light-emitting diodes (UV-LEDs) under a series of constant current stress. The failure mechanisms were investigated systematically by measuring the optical and electrical characteristics of the LEDs before and after aging. The variation of carrier concentration in the active region was analyzed by capacitance–voltage. Combining the extracted apparent charge distribution profiles with the simulation results of the devices before and after the stress, we found that the change of carrier concentration in the multiple quantum wells was related to the donor diffusion on the n-side. On the *p*-side, both the acceptor concentration of electron blocking layer (EBL) and the defects in *p*-GaN contact layer were also found to be under constant change. The reduction of the EBL doping concentration has contributed to an increase of the diode depletion width during the stress. The changes in the LEDs before and after stressing indicate a compensating effect occurred in the *p*-type EBL close to the quantum wells, which leads to the degradation of the optical power of the 265 nm UV-LEDs.

1 Introduction

Deep ultraviolet (DUV) light-emitting diodes (LEDs) based on AlGaN in the range of 200–280 nm (UV-C) are of high interest for several applications, including water purification and recycling, disinfection of medical equipment and food, UV curing, and plant growth lighting, due to their advantages of small size, low energy consumption, fast switching, and preheating time [1–5]. Compared with conventional mercury gas-discharge lamps, the exceptional characteristics of UV-LED devices, there are still technological difficulties, including the understanding of the degradation mechanisms, which limit the lifetime reliability and rapid market penetration of UV-C

Address correspondence to E-mail: czq8676@hotmail.com; ddjy2000@gmail.com; 20180001@gxu.edu.cn

https://doi.org/10.1007/s10854-021-06113-z

LEDs. Since the physical mechanisms responsible for degradation of UV-LEDs have not been completely identified, numerous researches have been conducted on the reliability analysis of UV-LEDs in recent years [6–10]. It is known that the threading dislocation densities (TDD) and poor ohmic contacts with high Al-content AlGaN layers lead to a mass of Joule heating and non-radiative recombination heating in the device during operation which accelerates degradation [11, 12]. On the other hand, the epitaxial growth conditions of AlGaN on the AlN buffer layer result in a relatively high density of point defects, such as III–V gallium vacancies, aluminum vacancies, and nitrogen vacancies (V_{Ga},V_{Al}, V_N) or hydrogen and carbon impurities [13–16], which will become Shockley–Read–Hall (SRH) recombination centers in the active region of the device and lead to lower internal quantum efficiency (IQE) [17–19]. Moreover, the point defects compensation by vacancies can limit the doping level, such as, V_{Ga} acts as acceptors and compensate *n*-type layer; V_N acts as single donors and compensate *p*-type layer, both of which decrease conductivity of the layers. Recently, many researchers suggested that during constant current stress both catastrophic and gradual degradation of output optical power (OP) can occur in UV-LEDs. Moe et al. considered that a compensating effect in the *p*-type electron barrier near the quantum wells occurred after aging [20]. Ruschel et al. presented a localization degradation method which made it possible to separate *p*-contact/*p*-side-related degradation effects from those of the active region [21]. The defect behaviors in the degradation of the AlGaN-based UV-C LEDs under constant current stress were systematically studied by Wang et al., who found that the degradation was mainly derived from the generation of V_{Ga} in the Si-doped region, as both the reduction of the output OP and the increase in the reverse current were linearly related to the increase in V_{Ga}[22].

In this paper, the degradation of AlGaN-based multiple quantum wells (MQWs) at 265 nm UV-C LEDs stressed by different constant currents (40 mA, 60 mA, 80 mA, 100 mA) was studied extensively, which could reveal detailed information on the nature of the operation current density involved in the degradation process. Combining capacitance voltage (C–V) measurements with simulations before and after different current stress provides the information on the change of carrier concentration of the active region and electron blocking layer (EBL) with respect to depth.

2 Experimental details

The investigation was performed on UV-C LEDs with a peak emission wavelength of 265 nm from the same wafer, which was grown by the metal–organic chemical vapor deposition (MOCVD) on the (0001) sapphire substrate. The growth started with an AlN layer, a 2-μm-thick Si-doped *n*-type AlGaN barrier layer and it was deposited on a high-quality AlN buffer layer. The main active region was three periods of 3-nm-thick $Al_{0.45}Ga_{0.55}$ N quantum wells (QWs), separated by 7-nm-thick $Al_{0.67}Ga_{0.33}$ N barriers (QBs). Then, a 60-nm-thick Mg-doped $Al_{0.85}Ga_{0.15}$ N EBL, followed by a 20-nm-thick Mg-doped $Al_{0.35}Ga_{0.65}$ N barrier layer, and a 0.15-μm-thick GaN cap layer. After growth, part of it was etched to the *n*-type AlGaN layer to facilitate the fabrication of the electrode. The *n*-type and *p*-type electrodes were deposited with Ti/Al/Ti/Au and Ni/Au. The standard mounted virgin LEDs had a peak emission wavelength of 265 nm.

In our study, the LEDs have standard encapsulation and are stressed at different current densities. The *n*-contact and *p*-contact of UV-LEDs were directly connected with the probe during aging and characteristic parameter testing to keep the output supply current stable and avoid interference from external factors. Before and after aging, the steady state photoluminescence (PL) spectra, optical power current (L–I), electroluminescence (EL) spectra, current voltage (I–V), and C–V were measured, respectively. The PL spectra were acquired by Raman spectrometer (LabRAM HR Evolution) with 325 nm laser unit. The C–V measurements were performed using a Keysight E4980A LCR Meter at a series of frequencies up to 1 MHz. During the operation, the input current, output OP and voltage, and temperature of the LEDs were measured continuously using a source meter (Keithley 2400), photodiode, and thermocouple thermometer. In order to further analyze the physical mechanisms of the degradation, the Simulator of Light Emitters based on Nitride Semiconductors (SiLENSe) was used to simulate the carrier distribution in the MQWs and the change of energy band structure [23]. All optical and electrical

characteristic parameter measurements were performed at room temperature.

3 Results and discussion

The LEDs were stressed with the currents from 40 mA, 60 mA, 80 mA, and 100 mA, which are in the current density range between 32.7 and 81.6 A/cm^2. Our current densities were consistent with other many studies and degradation curves were divided into catastrophic degradation and gradual degradation stages. The normalized OP during the stress are shown in Fig. 1. It can be observed from the aging curves that the OP decreased sharply with the increase of the injection current density in the first 30 min of the stress. For different current density levels, the optical decay rates were higher with higher currents.

The EL spectra of the LED before and after aging at various injection current are shown in Fig. 1 inset. The relative light intensity of the main emission peak at a low current (5 mA) decreased to 94%, 89%, 84%, 81%, respectively. The consistent peak indicated that the Al composition of the active region might not change and some new defects may be generated within or around the active region leading to more non-radiative recombination centers [24]. The I–V curves are shown in Fig. 2a, we detected an increase of leakage current in reverse and low forward-bias

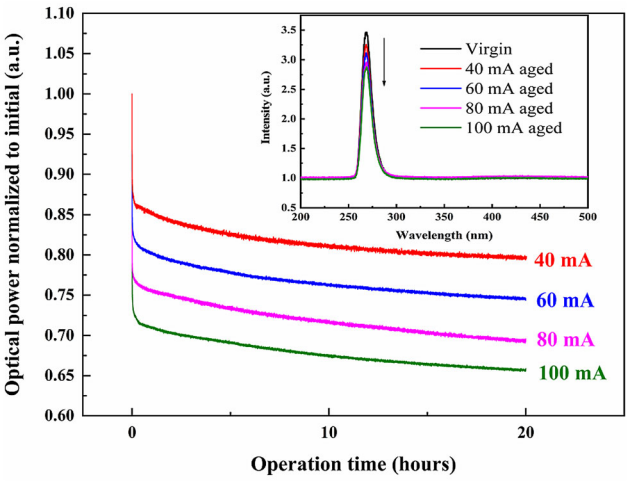

Fig. 1 The normalized OP of the UV-C LEDs stressed at a series of current of 40, 60, 80, 100 mA, respectively. Inset: The EL spectra were measured at 5 mA of the LEDs before and after aging at various injection current

region of the stressed devices. According to the previous study, the increase of the reverse-bias leakage current during operation could be caused by the increased defect density within or close to the active region, resulting in a higher number of point defect-assisted carrier transport and non-radiative recombination paths around the active layers. The forward-bias increased leakage current can be attributed to the defect-assisted tunneling process [22, 25–27]. Degradation may occur from the defect formation process induced by highly accelerated carriers flowing through the active region. Figure 2b shows the L–I curves for the LEDs before and after the stress. In the large measured current, the OP decreased with the increase of current stress, and the slope of the double-log coordinate L–I curves increased gradually, while in the small measurement current (< 1 mA), the slope of the curves decreased with the increase of the aging current. Combining the changes of forward voltage and ideal factors (at 20 mA) after different aging currents (Fig. S1), it can be concluded that the non-radiative recombination centers generated in the active region with the long-term continuous current injection. The faster the forward voltage decreased with the increase of the injection current, the more obvious the potential barrier decreased.

Compared to EL, PL measurement is non-invasive to the device and does not inject new carriers to affect the injection efficiency [28]. By analyzing the PL spectrum measured with a 325 nm laser, we can determine whether the *p*-type GaN produced new impurities or defects. It can be observed from Fig. 3 that the two peaks were significantly enhanced after stress. In previous studies, it has been suggested that the yellow luminescence enhancement at 2.4 eV was attributed to the generation of defects with relatively low formation energy at moderate temperature. A possible explanation for the enhancement is the easy diffusion of V_{Ga} and an oxygen atom sitting in a neighboring nitrogen site. Wang et al. proposed that after a consequence of current stress V_{Ga} was found to be generated in *p*-GaN layer by the departure of the unintentionally doped Mg from Mg_{Ga} along dislocation in the Si-doped region. These defects can partly compensate the unintentional *n*-type doping of the active region [22, 29–31].

The C–V performance was an important characteristic of LED *p*–*n* junction device. From C–V, we will be able to extract the width of the space charge region (SCR) and the amount of charge dependence

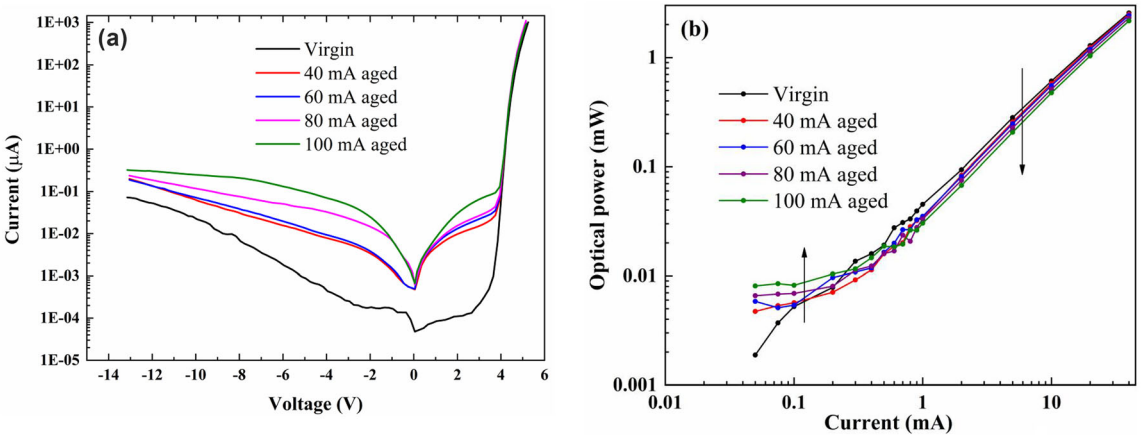

Fig. 2 **a** The I–V characteristics of the LEDs stressed at different currents. **b** The L–I characteristics were measured at a series of discrete currents

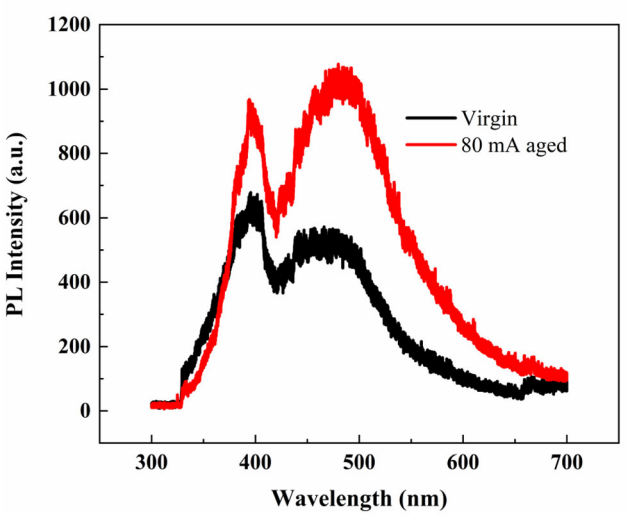

Fig. 3 The PL spectra of UV-C LED before and after electrical stress at room temperature

on the junction voltage, so the barrier capacitance was affected by the applied voltage. For non-compensated, uniformly doped semiconductor, assuming that N_D was the donor concentration of the material and fully ionized, the free carrier concentration was equal to the donor concentration. It is known from the theoretical studies that the C–V measurement concentration is approximately equal to the concentration of free carriers and satisfies the conservation of charge in heterojunction materials. The apparent charge distribution (ACD) and the depletion depth in the MQWs region can be calculated by the following formula [32]:

$$N_{CV} = N_D = n = \frac{C^3}{S^2 \varepsilon_0 \varepsilon_r q} \frac{dV}{dC} \tag{1}$$

$$W_D = \frac{S_{0r}}{C}, \tag{2}$$

where n is the free carrier concentration, C, S,ε_0, ε_r, q, and V are the capacitance, junction area, permittivity of vacuum, relative dielectric constant of the semiconductor, elementary charge, and voltage, respectively.

The above formulas were used for analyzing the carrier concentration and the relative location in the active region assuming unilateral junction, with the p-side much more heavily doped than the n-side. Hence the information of carrier distribution in the active region extracted from the C–V measurements was considered to be the n-side doping [20, 33, 34]. It was worth noticing that this assumption is an approximation in the determination of the apparent depths and carrier concentration, since the charge concentration at the p-side was limited, and the SCR usually extends on both the p and n sides. As shown in Fig. 4a, we performed the C–V measurement at 1 MHz before and after the device aging test. The capacitance decreased with the increase of aging current in the forward-bias range (0–5) V, which was consistent with Eq. (2) describing the voltage dependence of the capacitance as a function of the depletion width (W_D) of the p–n junction. The reduction of the maximum capacitance with increasing stress currents indicated that the depletion widths was larger than that of the virgin devices [7]. However, in the negative bias range (− 13–(− 2)) V,

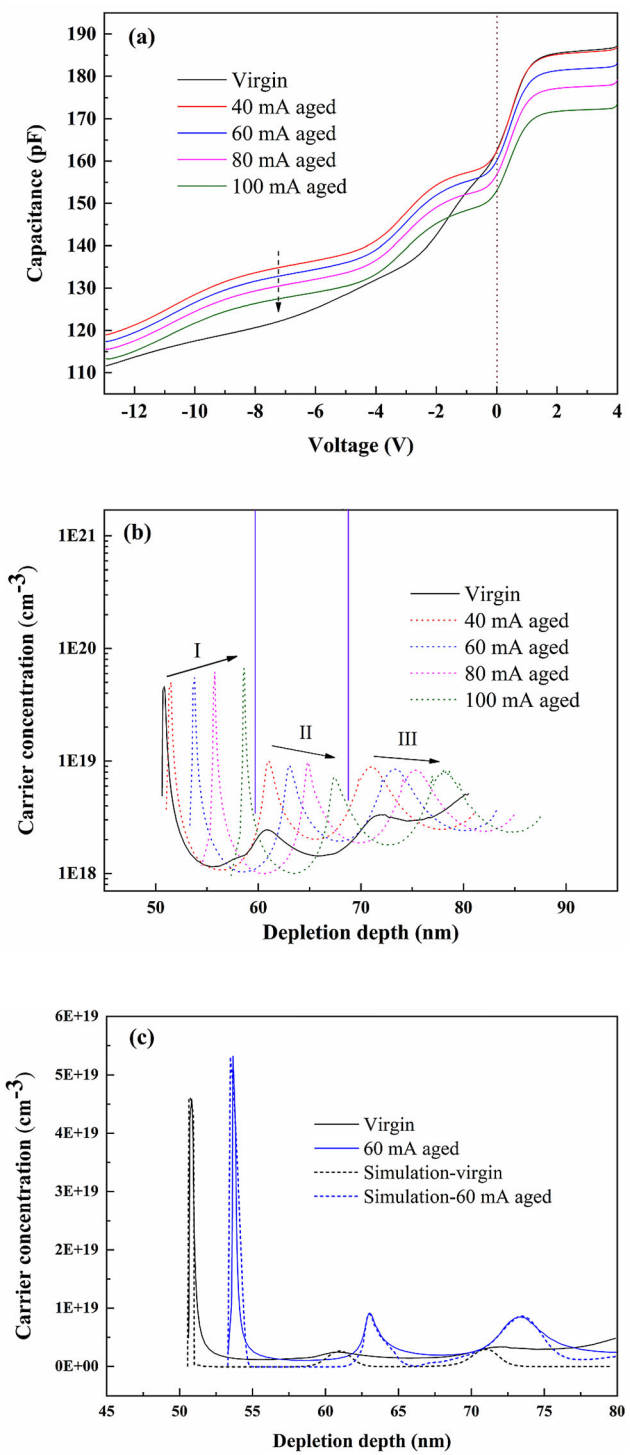

Fig. 4 **a** The C–V measurement results were at 1 MHz before and after the devices aging test. **b** The apparent charge distribution (ACD) profiles of unstressed and electrically stressed devices calculated from capacitance–voltage measurements with the frequency of 1 MHz, as a function of depletion depth. **c** The 1D simulation and test data of ACD profiles of original and stressed at 60 mA LEDs

after the device was injected with current and put through the same voltage ramp, the capacitance was much larger than that of the original device, indicating that stresses activated impurities and defects, and the capacitance decreased gradually with the increase of the aging current.

The ACD profiles of unstressed and electrically stressed devices were extracted from capacitance–voltage measurements with the frequency of 1 MHz, as a function of depletion depth. As shown in Fig. 4b, where the LEDs were aged with different currents, the carrier concentrations in QW II and QW III were significantly increased. It was also easy to observe that the carrier concentration of the main luminous QW I (the quantum well closest to EBL) increased with the increase of current stress and the depletion width of *p*-region. It indicated that the efficiency loss was probably related to the increase of non-radiative paths, due to the generation/propagation of defects in the active region closer to EBL, and more carriers were captured [33, 35]. However, the full width at half maximum of the QWs of II and III remained almost constant, the carrier concentration in the well decreased slightly with the increase of current stress, and with the increase of stress current, the boundary of depletion layer on the *p*-side moved from 50.79 nm to 51.43 nm, 53.81 nm, 55.71 nm, and 58.52 nm in sequence. The ACD profiles measured after stress indicated that long-time current injection induced localized modifications of the carrier redistribution in the active region, which could be ascribed to the generation of defective states on the basis of previous studies [33, 36]. After calculation, it was found that the increase of carrier concentration in the main emission peak of QW I was approximately equal to the sum of the decrease in QW II and QW III. Therefore, it can be inferred that donor-like impurities increased in each QW, and the carriers in QWs next to the n-side moved to p-side region after aging. If the current stress was increased, it can be found that the total impurities may no longer increase. The donor-like impurity defects of QW II and QW III propagated to the main luminescent QW I. The UV-LEDs stressed for a long-time result in carrier redistribution in the active region.

In order to further analyze the carrier distribution and the movement of depletion width of the degradation process of AlGaN-based LEDs, we used the SiLENSe 1D simulator to calculate the ACD profiles and energy band structure. The comparison between

the experimental and simulation results is shown in Fig. 4c. As can be seen from the consistency between the experiment and the simulation, our simulation structure can well explain the carrier distribution and the change of the depletion width before and after stress. It was found that the change of carrier concentration distribution was mainly related to the donor concentration in the quantum wells. We also observed that the change of depletion width was related to the acceptor concentration of the EBL. The extracted donor concentrations from the simulation of different aging stress currents were compared in Fig. 5a and normalized to the values of virgin device. For the *n*-side MQWs region, different QWs correspond to different changes. The donor concentration of the first QW near the *p*-side was always increasing, while for the other two QWs, the donor concentration firstly increased rapidly and then decreased slowly. In combination with the ACD file extracted from the experiment, it could be seen that the experimental and simulation results of each QW change behavior were consistent. Donor-like defects could be formed in or around the active region by current activated diffusion, as we also observed in the degradation process of 280 nm LEDs (Su et al.) [6]. For example, substituting gallium (C_{Ga}) was a commonly observed impurity in III-nitride layers, Miceli et al. proposed that V_N, $Mg_{Al}-V_N$, and $Mg_{Ga}-V_N$ complex could result in a self-compensation effect with hybrid density functional theory [37, 38]. These defects compensated the *p*-type doping of EBL and served as non-radiative recombination centers, resulting in the OP reduction. With the decrease of acceptor concentration of the EBL, the depletion width of the *p*-side was widened.

For further study the increase in the width of the *p* depletion layer by a reduced acceptor concentration of the EBL in more detail, self-consistent simulations based on an one-dimensional drift–diffusion model and solved the Schrödinger, Poisson, and continuity equations with proper boundary conditions. The calculated band diagram and electric field distribution have been performed. In our simulation, we considered polarization charges at the interface of QW/EBL junction and varied the acceptor concentration of EBL to simulate the broadening of the p depletion region. The total change of the calculated energy band structure and the simulation schematic diagram of AlGaN-based LEDs are shown in Fig. 5b

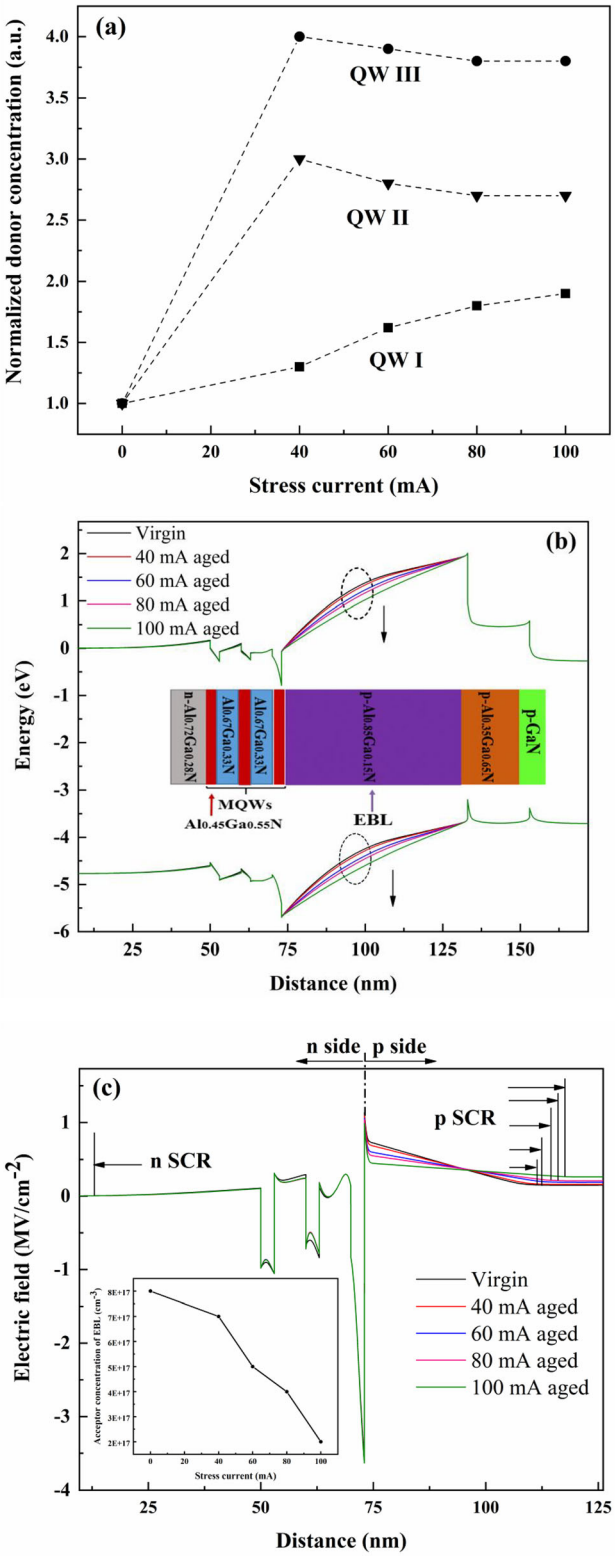

◀**Fig. 5** **a** The normalized donor concentration of degradation simulation with different stressed currents. **b** The band diagram of virgin and different stress currents aged structure simulations. Inset: The simulation structure of AlGaN-based UV-LEDs. **c** The calculated electric field distribution around the p–n junction of the simulation structure for different conditions. Inset: The acceptor concentration of EBL at different stress currents

and inset of Fig. 5b. It was indicated that the energy of the EBL decreased gradually with the change of the doping of the EBL. The electric field distribution around the *p*–*n* junction of the simulation structure for different conditions and the acceptor concentrations of the EBL are shown in Fig. 5c and inset of Fig. 5c. From the energy band diagram and the distribution of electric field, it can be found that the variation of the depletion width occurs in the *p*-side, while the depletion width almost remains constant at the *n*-side. The edge of the *p* depletion layer was the position where the slope of the electric field reached zero. It can be seen from the simulation results that the edge of *p* SCR moved 1.08, 3.03, 4.89, 7.24 nm to the *p*-region, which was almost consistent with the ACD profiles in the experiment. Our results indicated the expansion of the depletion region due to the EBL acceptor concentration change, in addition to a donor diffusion process across the MQW region as suggested by Glaab et al. [7]. We believe that the lack of a very high Al interlayer may contribute to the difference of the simulation results. Also, our results at more negative biases, which are needed to deplete the different quantum wells, strongly suggested that the main expansion of the depletion region are from the acceptor diffusion in the *p*-type EBL. Preliminary analysis indicates that the EBL acceptor concentration reduction, as indicated in the inset of Fig. 5c, will lead to lower hole density and higher electric field inside the MQW, especially the first quantum well, at higher current, compared to virgin device. Similar to the results in [39], the lower hole density is corresponding to lower hole injection efficiency and radiative recombination rates at higher current. Thus, we believe the acceptor diffusion contributes to the device degradation under stress.

4 Conclusions

In summary, degradation mechanisms of AlGaN-based 265 nm UV-C LEDs under a series of constant currents stress were systematically studied with I–V, C–V, power measurements, and 1D simulations. By comparing the experimental and simulation carrier concentration of the virgin and aged devices, we found that the changes of the EBL acceptor concentration at different stress currents lead to various depletion widths on the *p*-side of the diode, instead of a simple *n*-side donor diffusion process as reported in the previous literature. The increase of the defect density was verified by *p*-GaN material characterization. Both of these two mechanisms may cause lower hole injection rate at higher stress currents, which explains the more dramatic degradation of the 265 nm UV-LED compared to diodes emitting at 280 nm or longer wavelengths. On the other hand, our simulation results also indicate the donor diffusion process inside the QWs, both of which can play a major role in the further optical power degradation. Thus, future efforts to enhance the EBL stability and hole injection rate is important for the commercial UV-LED epitaxy structure design.

Acknowledgements

This work was supported financially by the fund for Bagui Talent of Guangxi Province (No. T3120097921, Nos.T31200992001), Talent Model Base (AD19110157), Guangxi Science and Technology Program (AD19245132), Guangxi University Foundation (A3120051010), and Guangxi Science and Technology Base and talent Special project (AD20238093).

Declarations

Conflict of interest There are no conflict to declare.

Supplementary Information: The online version contains supplementary material available at https://doi.org/10.1007/s10854-021-06113-z.

References

1. D. Lee, J.W. Lee, J. Jang et al., Appl. Phys. Lett. **110**, 191103 (2017)

2. M. Kneissl, T.-Y. Seong, J. Han, H. Amano, Nat. Photonics **13**, 233–244 (2019)
3. M. Schreiner, J. Martínez-Abaigar, J. Glaab, M. Jansen, Optik Photonik **9**, 34–37 (2014)
4. D. Monti, M. Meneghini, C. De Santi et al., IEEE T Electron Dev. **64**, 200–205 (2016)
5. S. Vilhunen, H. Särkkä, M. Sillanpää, Environ. Sci. Pollut. Res. **16**, 439–442 (2009)
6. M. Su, X. Zhu, Q. Guo et al., AIP Adv. **11**, 035315 (2021)
7. J. Glaab, J. Haefke, J. Ruschel et al., J. Appl. Phys. **123**, 104502 (2018)
8. J. Glaab, C. Ploch, R. Kelz et al., J. Appl. Phys. **118**, 094504 (2015)
9. J. Ruschel, J. Glaab, F. Mahler, T. Kolbe, S. Einfeldt, J.W. Tomm, Appl. Phys. Lett. **117**, 121104 (2020)
10. J. Glaab, J. Ruschel, F. Mehnke et al., Semicond. Sci. Tech. **33**, 095017 (2018)
11. M. Lapeyrade, S. Alamé, J. Glaab et al., J. Appl. Phys. **122**, 125701 (2017)
12. Z. Gong, M. Gaevski, V. Adivarahan, W. Sun, M. Shatalov, M. Asif Khan, Appl. Phys. Lett. **88**, 121106 (2006)
13. C.G. Van de Walle, J. Neugebauer, J. Appl. Phys. **95**, 3851–3879 (2004)
14. A.Y. Polyakov, I.-H. Lee, Mat. Sci. Eng. R **94**, 1–56 (2015)
15. M. Auf, B. der Maur, I Pietzonka Galler, M. Strassburg, H. Lugauer, A. Di Carlo, Appl. Phys. Lett. **105**, 133504 (2014)
16. A. Wright, J. Appl. Phys. **92**, 2575–2585 (2002)
17. S.Y. Karpov, Y.N. Makarov, Appl. Phys. Lett. **81**, 4721–4723 (2002)
18. N. Susilo, S. Hagedorn, D. Jaeger et al., Appl. Phys. Lett. **112**, 041110 (2018)
19. M. Akiba, H. Hirayama, Y. Tomita, Y. Tsukada, N. Maeda, N. Kamata, Phys. Status Solidi C **9**, 806–809 (2012)
20. C.G. Moe, M.L. Reed, G.A. Garrett et al., Appl. Phys. Lett. **96**, 213512 (2010)
21. J. Ruschel, J. Glaab, M. Brendel et al., J. Appl. Phys. **124**, 084504 (2018)
22. Y.-Z. Wang, X.-F. Zheng, J.-D. Zhu et al., Appl. Phys. Lett. **116**, 203501 (2020)
23. Simulator of Light Emitters based on Nitride Semiconductors SiLENSe 5.14 (STR Group website. http://www.str-soft.com/learn/InAlGaN_Alloys/index.htm).
24. Q. Shan, D.S. Meyaard, Q. Dai et al., Appl. Phys. Lett. **99**, 253506 (2011)
25. E. Jung, J.K. Lee, M.S. Kim, H. Kim, IEEE Trans. Electron. Dev. **62**, 3322–3325 (2015)
26. P. Dalapati, K. Yamamoto, T. Egawa, M. Miyoshi, Opt. Mater. **109**, 110352 (2020)
27. S. Lee, D. Oh, H. Goto et al., Appl. Phys. Lett. **89**, 132117 (2006)
28. M. La Grassa, M. Meneghini, C. De Santi et al., Microelectron. Reliab. **55**, 1775–1778 (2015)
29. M.A. Reshchikov, H. Morkoç, J. Appl. Phys. **97**, 5–19 (2005)
30. S. Limpijumnong, C.G. Van de Walle, Phys. Rev. B **69**, 035207 (2004)
31. M. Meneghini, D. Barbisan, L. Rodighiero, G. Meneghesso, E. Zanoni, Appl. Phys. Lett. **97**, 143506 (2010)
32. O. Ambacher, J. Smart, J. Shealy et al., J. Appl. Phys. **85**, 3222–3233 (1999)
33. F. Rossi, M. Pavesi, M. Meneghini et al., J. Appl. Phys. **99**, 053104 (2006)
34. M. Lucia, J. Hernandez-Rojas, C. Leon, I. Mártil, Eur. J. phys. **14**, 86 (1993)
35. Z. Ma, H. Cao, S. Lin, X. Li, L. Zhao, Solid State Electron. **156**, 92–96 (2019)
36. M. Meneghini, M. Pavesi, N. Trivellin, R. Gaska, E. Zanoni, G. Meneghesso, IEEE Trans. Device Mat. Reliab. **8**, 248–254 (2008)
37. G. Miceli, A. Pasquarello, Phys. Rev. B **93**, 165207 (2016)
38. Z. Ma, A. Almalki, X. Yang et al., J. Alloy. Compd. **845**, 156177 (2020)
39. Y.-K. Kuo, J.-Y. Chang, F.-M. Chen, Y.-H. Shih, H.-T. Chang, IEEE J. Quantum. Elect. **52**, 1–5 (2016)